

<https://doi.org/10.1038/s40494-025-02205-9>

Investigating subsidence characteristics of Kyoto imperial garden cultural heritage shaped by historical landscape construction, through remote sensing

Check for updates

Jingshu Cui¹, Yongxuan Ran², Xie Hu², Shiro Takeda¹, Junhua Zhang¹, Shan Cui³, Kwangmin Ham⁴, Xinyan Huang¹ & Fuham Sun¹

The Kyoto imperial gardens, regarded as “second nature” shaped by human transformation of the natural environment, include four of the most representative sites that serve as exemplary cases for land subsidence research. Analyzing subsiding characteristics is crucial for effective conservation. This study utilized time series Interferometric Synthetic Aperture Radar (InSAR) to analysis and verified with GNSS data. Further investigations of the construction methods and garden history revealed: Sites whose foundations follow traditional Kyoto-palace practices may be susceptible to subsidence due to their placement within of thin Holocene sedimentary deposits; Landscapes constructed through lake excavation, hill construction, and stonework, may experience subsidence caused by thick Holocene deposits; Gardens following natural topography may undergo land deformation due to groundwater and pore pressure redistribution. This study integrates traditional construction and remote sensing, offering a reference framework for the monitoring and protection of heritage.

Japanese gardens are artistic reproductions of natural landscapes, abstracted, compressed, and reimagined through human design to create a symbolic “second nature”¹. Kyoto imperial gardens exemplify this expression of Japanese garden art, with the Kyoto Imperial Palace, Sento Imperial Palace, Katsura Imperial Villa, and Shugakuin Imperial Villa regarded as the most artistically significant examples. Their design is rooted in the clean and orderly aesthetics of native Japanese garden traditions, often featuring meticulously arranged gravel surfaces that symbolize Kyoto traditional culture². Among the four imperial gardens, the Kyoto Imperial Palace and the Sento Imperial Palace represent the pinnacle of palace architecture and construction culture. Katsura Imperial Villa is regarded as the consummate example of the Japanese garden tradition of lake excavation and hill construction, whereas Shugakuin Imperial Villa fully utilizes natural terrain and mountain rocks for scenic composition. Collectively, these four imperial gardens represent the culmination of Japanese traditional garden construction methods and embody significant historical and cultural value³.

Beneath the uniquely refined landscapes shaped by construction methods such as lake excavation, hill construction, stone paving, and traditional architectural techniques, land subsidence may emerge in imperial

garden cultural heritage. Like historic gardens around the world, these sites are subject to historical changes, groundwater redistribution, and intense rainfall, which contribute to long-term process of ground destabilization in garden cultural heritage^{4,5}. Most garden cultural heritage worldwide require major restoration every seven to ten years⁶. The restoration reports suggest structural damages, where the external steels and ropes have often been used to stabilize buildings. As part of the restoration, collapsed or leaning retaining walls were replaced and damaged pavement was repaired. Current restoration and routine maintenance policies prioritize the use of locally sourced, natural, and traditional materials while minimizing or avoiding modern substances, such as steel nails and concrete. This approach aims to sustain traditional landscape construction methods and maintain the historical atmosphere^{7,8}. This approach follows a commitment to craftsmanship and sustainability. Regular inspections and maintenance are indispensable^{9,10}. These gardens have a history spanning nearly 400 years. The spatial characteristics of land subsidence within Kyoto imperial garden cultural heritage remain unclear.

Traditional methods for investigating garden heritage land subsidence often involve the use of settlement markers applied to measuring scales on

¹Graduate School of Horticulture, Chiba University, Matsudo, Japan. ²College of Urban and Environmental Sciences, Peking University, Beijing, China. ³Graduate School of Horticulture, China Agricultural University, Beijing, China. ⁴Department of Environmental Landscape Architecture, Gangneung-Wonju National University, Gangneung, South Korea. e-mail: 23hd0502@student.gs.chiba-u.jp

concealed wooden columns of historic buildings. Sensors have been used in some cases and offer a flexible approach^{11,12}. However, in-situ inspection is labor-intensive and time-consuming, and its effectiveness is limited by the need for discrete measurements. In addition, installing monitoring equipment may pose a risk of physical disturbance to the garden heritage environment¹³. Reliance on manual methods also introduces delays, as protective measures are often implemented only after visible cracks appear in landscape structures, thereby increasing the complexity and cost of repair¹⁴. In contrast, Interferometric Synthetic Aperture Radar (InSAR) is an advanced observation technique. By transmitting and receiving radar signals and calculating the phase differences between radar images acquired at different times or from different viewing angles, InSAR enables precise measurement of ground deformation¹⁵. Numerous previous studies have demonstrated agreement between InSAR-derived displacement measurements and leveling data, with reported annual errors on the order of centimeter to millimeter scale per year^{16,17}. High-coherence InSAR pixels are often concentrated on artificial landscape features such as building rooftops, building corners, courtyard pavements, rigid retaining walls, and rockeries. This spatial distribution provides a valuable opportunity to detect land deformation of the man-made structures of historical gardens. The potential of remote sensing in cultural heritage research has recently gained increasing attention, as it enables quantitative monitoring and assessment. In regions with cultural heritage sites—such as China, Myanmar, and Italy—InSAR techniques have been employed to detect areas of long-term, gradual ground deformation^{18–21}. Xu et al. employed InSAR to detect land deformation features of the Badaling Great Wall in China and noted that the deformation rate was higher at the southwest of the beacon tower, where cracks and damaged facilities were also observed¹⁸. Zhou et al. used the SBAS-InSAR and PS-InSAR methods to demonstrate that several monuments were experiencing significant subsidence in the Bagan cultural heritage site in Myanmar and analyzed the causes of ground deformation²⁰. Chen et al. used ascending Sentinel-1 images to detect land deformation features of cultural heritage sites along the Silk Road in China and noted that the Wei Yang Palace and the Xuanzang Pagoda were sinking²². However, current methods for monitoring heritage deformation are often limited to one-dimensional measurement and frequently lack ground-truth validation (e.g., GNSS data). Integrating InSAR observations and ground-based measurements is therefore essential for accurately analyzing land subsidence in cultural heritage contexts.

In this research, the multi-track SBAS-InSAR approach is applied in combination with ground-truth validation to monitor ground deformation in the Kyoto imperial gardens. Integrating data from both ascending and descending tracks densifies the measurements, while the Small Baseline Subset (SBAS) InSAR approach—using small temporal-spatial baseline pairs to generate displacement time series—is particularly well suited for monitoring ground deformation in historical gardens. The derived InSAR products, including ground deformation velocities and time series, allow us to identify subsidence zones in four major imperial gardens. In this research, the primary causes of subsidence in these areas are inferred based on landscape construction techniques, geological conditions, and hydrological environments. No prior study has linked traditional Japanese garden construction techniques to spatial patterns of land subsidence. The results indicate that remote sensing can effectively detect land subsidence areas and deformation trends in garden cultural heritage, particularly when conventional methods such as field surveys are unavailable.

Methods

Study area and data acquisition

This study focuses on the four most renowned imperial gardens in Kyoto, including (1) the Kyoto Imperial Palace (Fig. 1a), which has a garden history dating back to 749 CE. Most of its current structures were reconstructed after the fire of 1855, and the site now spans 110,000 m²; (2) the Sento Imperial Palace (Fig. 1b), initiated in 1630 under imperial directive, was reconstructed after the 1855 fire, and currently covers an area of 89,000 m²; (3) the Katsura Imperial Villa (Fig. 1c), located adjacent to the Katsura River,

was originally built under the direction of Prince Toshihito between 1620 and 1624. It underwent multiple expansions and modifications and currently spans ~70,000 m²; and (4) the Shugakuin Imperial Villa, located in a former aristocratic estate area, forms part of the scenic mountainous outskirts of Kyoto. Constructed between 1656 and 1659 under the direction of Emperor Go-Mizunoo, the villa's buildings and landscape largely preserve their original 17th-century appearance (Fig. 1d). The site currently covers an area of ~540,000 m². Collectively, these four imperial gardens represent the culmination of imperial garden landscape construction art and embody significant historical and cultural values. Traditional buildings within gardens are primarily timber-framed and constructed using materials such as earth, thatch, and stones. These structures typically rest on shallow foundations²³. Large artificial hills are commonly created by piling soil excavated during lake construction. Another prevalent method involves utilizing gentle foothill slopes at the base of the mountains surrounding the Kyoto Basin to integrate them into the landscape design. Historically, garden water features were fed by nearby river systems, whereas in modern times they are mostly sustained by groundwater sources.

Imperial gardens were primarily distributed within the Kyoto Basin and on adjacent mountain slopes along its edges. The basin is surrounded by mountains on the north, west, and east sides, forming a basin that opens to the south. The Kyoto region exhibits a distinct north–south geological contrast: its northern part is characterized by widespread distributions of Paleozoic shale and siliceous rock, with sediments predominantly composed of fine-grained clay, as in the areas where the imperial gardens examined in this study are located (Fig. 1B). Summers in Kyoto are hot and oppressively humid, while winters are cold, windy²⁴. Kyoto is characterized by a prolonged rainy season, as well as frequent convective storms during summer, and active typhoon seasons in summer and autumn often bring episodes of extreme rainfall²⁵. Overall, the climate is persistently humid through the year (Fig. 1). This geological heterogeneity, combined with concentrated rainfall events have been considered potential factors influencing localized ground deformation characteristics in Kyoto^{26,27} (Fig. 2).

As garden cultural heritage that have long been exposed to frequent human-induced and natural disturbances, sustainable preservation of the existing remains is a primary task. To monitor landscape deformation, this study utilizes 133 ascending-track and 151 descending-track C-band SLC SAR images acquired by the European Space Agency's Copernicus Sentinel-1 satellite between 2017 and 2022. All images were collected in Interferometric Wide Swath (IW) mode with VV polarization (Table 1 and Supplementary Table S1). The temporal acquisition interval was ~12 days. The spatial resolution of the IW-mode imagery was ~5 m in the range direction and 20 m in the azimuth direction.

In the InSAR data interpretation process, external DEM data play a crucial role in simulating and removing topographic phase components. The SRTM1 DEM was used for topographic correction²⁸. Additionally, the precise orbit products were utilized to correct long-wavelength phase ramps due to minor orbital shifts. High-resolution data such as TerraSAR-X are not openly available and are often less frequently collected. Here we incorporated ascending and descending Sentinel-1 data to enhance the temporal resolution of ground deformation monitoring and our investigations of garden cultural heritage^{22,29}.

SBAS-InSAR multi-track processing and validation workflow

The methodology comprised four primary steps to generate and validate the SBAS multi-track deformation results (Fig. 3). First, SBAS processing was applied separately to the SAR data from both ascending and descending tracks, deriving results from different viewing geometries to enhance the robustness of the analysis and to perform repeatability checks. Second, line-of-sight (LOS) displacement measurements derived from the SBAS results were decomposed into two-dimensional displacement components. Third, the accuracy of the model was evaluated using the root mean square error (RMSE) as a statistical metric, and GNSS external data were employed as a control for reliability validation. Finally, the displacement results were interpreted in conjunction with traditional landscape construction

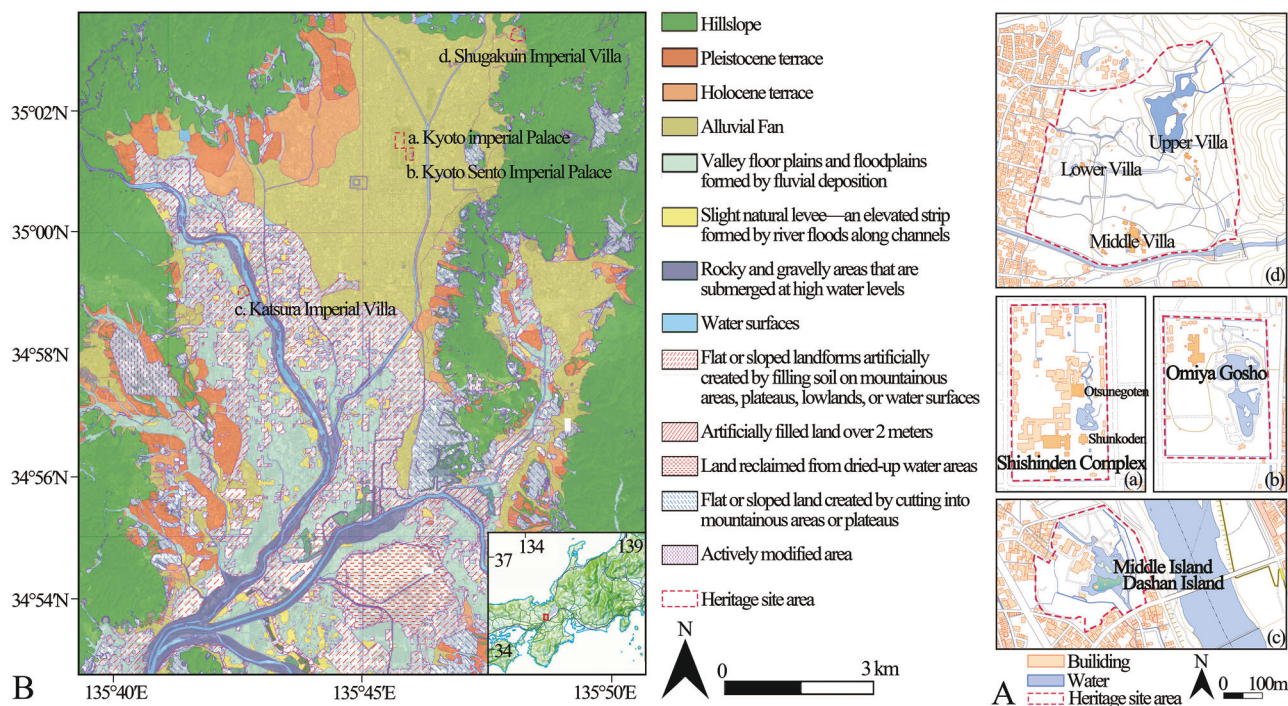


Fig. 1 | Layout and geographical context. **A** Layout plans of the four imperial gardens in Kyoto. **B** Locations of the four imperial gardens in Kyoto and analysis of the surrounding geographical environment.

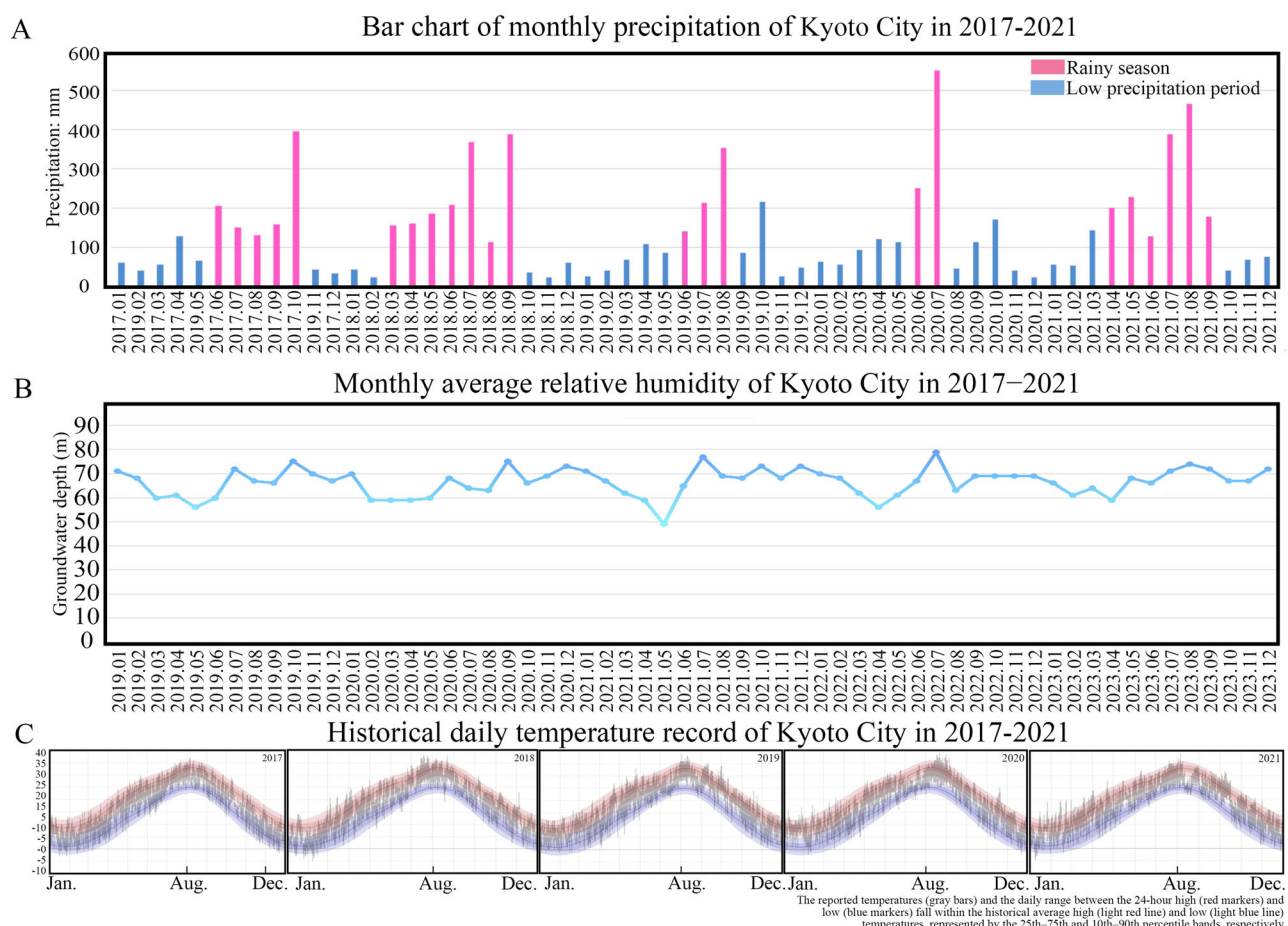


Fig. 2 | Climatic conditions of Kyoto City in 2017–2021. **A** Monthly precipitation. **B** Monthly average relative humidity. **C** Historical daily temperature record.

techniques, supported by field survey findings, official management reports, and relevant hydrological data. The entire workflow relies on freely available Sentinel-1 data and standardized processing methods, ensuring the reproducibility.

InSAR processing

InSAR technology derives ground displacement measurements from phase information in SAR images. The Sentinel-1 satellites acquire single-look-complex (SLC) SAR images over the same area in repeat-pass orbits. The

geometric differences between the two satellite acquisitions result in an interferometric phase difference. This phase difference is a combination of the topographic contribution and any surface displacement along the LOS direction. By removing the topographic phase (e.g., using a digital elevation model), the residual phase can be derived and converted into LOS displacement³⁰.

SBAS-InSAR processing constructs a network of interferograms from multiple SAR acquisitions. First, all the SAR images were grouped into small baseline subsets based on predefined thresholds of temporal and perpendicular baselines (e.g., 60 days and 300 m in this study) to minimize decorrelation. The processing algorithm then automatically selects a super master image as the common reference scene for each subset, and all interferometric pairs are co-registered to it. Using GAMMA software, 525 and 642 interferometric pairs were generated for the ascending and descending tracks, respectively, under these baseline constraints. In vegetated environments such as gardens, paddy fields, and forested areas, Sentinel-1 SBAS interferograms often experience severe decorrelation when the temporal baseline exceeds 2–3 months^{31–33}. Therefore, in this study, the temporal baseline was limited to 60 days to ensure network connectivity and the stability of the time series results. A perpendicular baseline threshold of 300 m was adopted to minimize geometric decorrelation. These settings collectively help maintain reliable coherence and improve the accuracy of deformation estimates.

Figure 4 illustrates the spatial and temporal baseline of SAR images from (A) the ascending track and (B) the descending track, acquired between 2017 and 2021. Compared to other time series InSAR techniques, SBAS-InSAR is characterized by its ability to process multiple interferometric pairs, provided that their temporal and spatial baselines remain within predefined thresholds, allowing for their visualization in phase space. To enhance the signal-to-noise ratio (SNR) and spatial resolution, we adopted a minimum multi-looking factor of 4:1 in the range and azimuth directions. This configuration significantly improves the SNR while maintaining relatively high spatial resolution, thereby preserving the coherence of the interferometric phase as much as possible³⁴.

To ensure the reliability of the deformation inversion, this study employed thresholds for average coherence and temporal coherence as criteria for selecting coherent targets (CTs). Average coherence is a key

Table 1 | Basic parameter information of experimental data

Dataset	Parameters	Information
Sentinel-1B	Orbit	ASC
	Path	10
	Frame	107
	Temporal span	05/01/2017–22/12/2021
	N of data	133
	Polarization	VV
	The angle of incidence (°)	40.2907
Sentinel-1A	Heading angle (°)	-13.0364
	Orbit	DES
	Path	17
	Frame	474
	Temporal span	23/01/2017–09/01/2022
	N of data	151
	Polarization	VV
SRTM1	The angle of incidence (°)	37.6840
	Heading angle (°)	-167.0662
AUX_POEORB	Elevation datum	WGS84/EGM96
	Resolution (m)	30
AUX_POEORB	Positioning accuracy (cm)	5

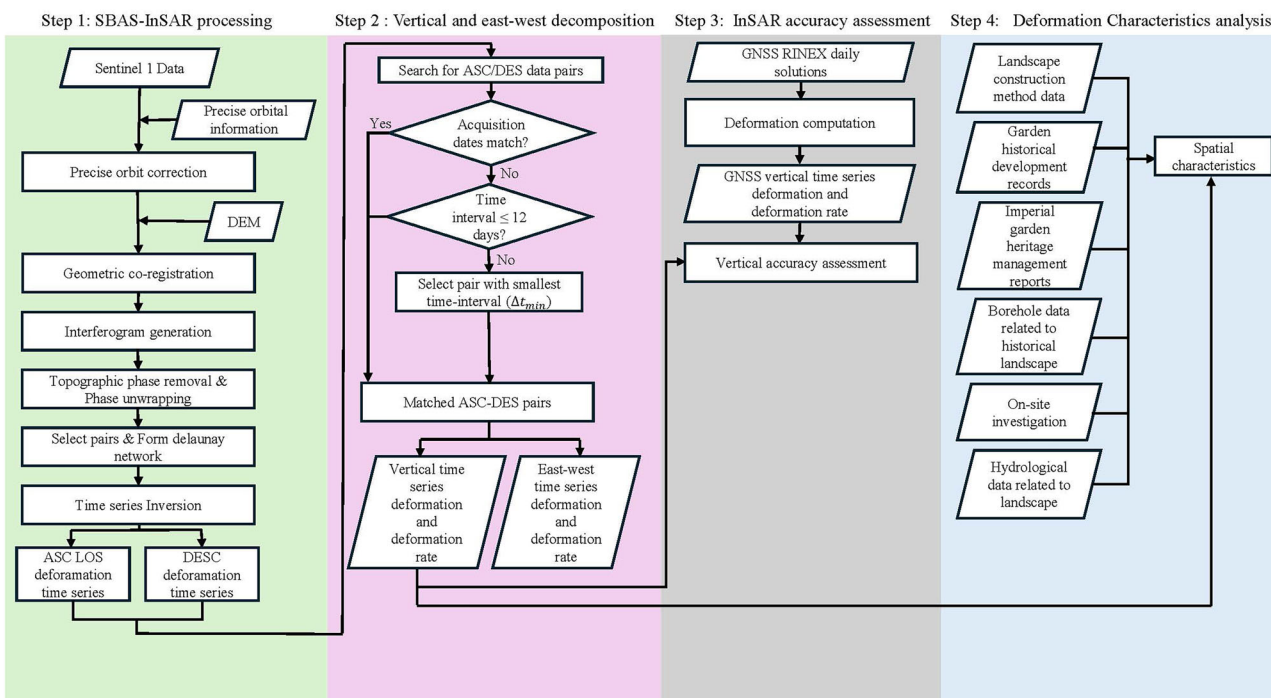


Fig. 3 | Four primary stages of vertical displacement analysis using two-dimensional (2D) decomposition.

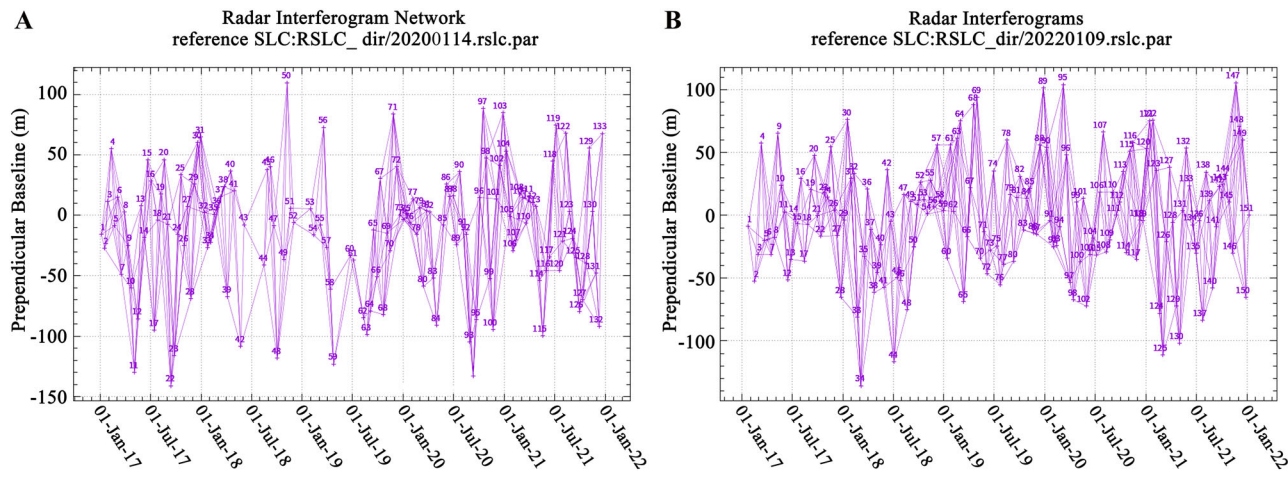


Fig. 4 | Spatial and temporal baseline plots of SAR images. A ascending-track. **B** descending-track InSAR data.

indicator used in the SBAS method for identifying CTs because it quantifies the overall coherence level of a given pixel across multiple interferograms:

$$\gamma_{av} = \frac{1}{N} \sum_{i=1}^N \gamma_i$$

where γ_{av} represents the average coherence of a pixel over the entire time series, N is the total number of interferograms in which the pixel appears, and γ_i is the coherence of the pixel in the i^{th} interferogram. In this study, pixels with an average coherence below the threshold of 0.3 were removed to eliminate low-coherence areas significantly affected by noise, such as water bodies and densely vegetated areas, ensuring that the selected targets maintain high spatial coherence across multiple interferograms. Additionally, a temporal coherence threshold of 0.3 was applied as a further criterion for selecting CTs. This step help exclude pixels with unstable phase variations in the time series while ensuring sufficient CTs across a large spatial extent³⁵.

Ferretti et al. pointed out that the choice of coherence threshold requires a balance between spatial coverage and accuracy, and that overly high thresholds may result in the loss of critical area information^{36,37}. In this study, the temporal coherence threshold was relaxed to 0.3 to increase the spatial density of measurements over landscapes. This setting has already been adopted in SBAS studies related to garden culture heritage^{20,38,39}.

Displacement decomposition

InSAR observations yields deformation measurements along the LOS direction, which is geometrically defined by the incidence angle (θ) and the satellite heading angle (α):

$$v_{los} = (-\sin \theta \cos \alpha \sin \theta \sin \alpha \cos \theta) \begin{pmatrix} v_{UD} \\ v_{EW} \\ v_{NS} \end{pmatrix} \quad \text{where } v_{UD} \text{ represents}$$

the vertical velocity, and v_{EW} represents the horizontal velocity component in the east–west direction. Because most current SAR satellites operate in near-polar orbits and are insensitive to along-track (north–south) deformation, the north–south component, v_{NS} , is usually neglected in spaceborne InSAR solutions³⁸. When only a single-track InSAR dataset is available, horizontal displacement is often disregarded, and the LOS deformation results are directly projected onto the vertical direction⁴⁰:

$$v_{UD} = \frac{v_{los}}{\cos \theta}$$

However, this approach may introduce inaccuracies by ignoring the horizontal deformation component. Although most of the study areas consist of flat, low-lying areas with gentle slopes, deformation predominantly occurs in the vertical direction. When at least two SAR

observations from different viewing geometries (e.g., ascending and descending tracks) are available, the following system of equations can be established⁴¹:

$$\begin{pmatrix} v_{asc} \\ v_{dec} \end{pmatrix} = \begin{pmatrix} -\sin \theta_{asc} \cos \alpha_{asc} \cos \theta_{asc} \\ -\sin \theta_{des} \cos \alpha_{des} \cos \theta_{des} \end{pmatrix} \begin{pmatrix} v_{UD} \\ v_{EW} \end{pmatrix}$$

where v_{asc} and v_{dec} represent the LOS velocity from the ascending and descending tracks, the incidence angles θ are 40.290° and 37.687° for the ascending and descending tracks, and the satellite heading angles α are -13.036° and -166.934° , respectively (Table 1).

Temporal disparities in data acquisition across satellite platforms pose a challenge when applying this two-dimensional framework to time series analysis⁴². To address this, the present study adopted a nearest acquisition interval method for time series processing, as detailed in the workflow illustrated in Fig. 3. The process begins by searching data pairs with the same acquisition dates. When such pairs are identified, the time series can be decomposed accordingly. If no such pairs are found, the search continues for the data pairs with the smallest acquisition interval⁴³. Given the 12-day revisit cycle of Sentinel-1, the first matching loop was constrained to search for data pairs with a time interval of no more than 12 days, where the date difference (Δd_{\min}) was minimized—ideally as close to 0 as possible—and did not exceed the revisit period T . In the second loop, this constraint was relaxed to include data from tracks with different revisit intervals, aiming to identify the pair with the smallest Δd_{\min} across the entire dataset, independent of T . Spatial alignment between ascending and descending data was performed using the nearest-neighbor co-location method, which is appropriate for heritage site assessment⁴⁴.

Additionally, since Sentinel-1 InSAR measurements are generally more sensitive to vertical deformation than horizontal motion, previous studies have shown that its vertical error is typically smaller than its east–west error^{26,43,45}. This study primarily focused on the vertical displacement component in the subsequent analysis.

Global Navigation Satellite System (GNSS) data processing

GNSS provides high-precision deformation positioning, velocity, and time series. In this study, GNSS data from all available stations in Kyoto provided by the Nevada Geodetic Laboratory were used to evaluate the accuracy of the vertical results derived from SBAS-InSAR. Blewitt et al. provided processed GNSS station displacement estimates and the associated time series data⁴⁶. In this research, the accuracy of the vertical velocity derived from InSAR measurements is evaluated. To ensure a valid comparison of the vertical deformation, the period from 2017 to 2021 — during which both GNSS and InSAR data were available — was selected as the comparison window. For each GNSS station, InSAR measurement points located within a 50-meter

radius were spatially averaged to estimate the deformation at that location. All GNSS stations were in areas with sufficient InSAR data coverage⁴⁷.

The vertical component (Up) of the GNSS time series and the corresponding vertical time series from SBAS-InSAR were processed using weighted least-squares linear fitting to derive the vertical deformation velocity over the period 2017–2021. The RMSE between the two datasets was calculated:

$$\text{RMSE} = \sqrt{\frac{1}{n} \sum_{i=1}^n (y_i - \hat{y}_i)^2}$$

Results

InSAR monitoring results

Using the SBAS-InSAR method, deformation velocities of the Kyoto imperial garden heritage site and its surrounding areas were estimated. Figure 5A, B shows the predicted vertical velocities from the ascending and descending tracks, respectively. Figure 5C presents the vertical velocity component obtained through the decomposition of LOS velocities, whereas Fig. 5D illustrates the horizontal velocity component in the east–west direction. Throughout the results, positive values indicate eastward and upward motions, and negative values represent westward and downward movements.

The deformation results indicated that most areas remained stable (Fig. 5). Consistent with previous findings in heritage site monitoring^{20,48}, high-coherence pixels in the SBAS-InSAR results are typically concentrated on hard artificial features; areas covered by vegetation, water surfaces, or loose soil exhibit low coherence due to severe spatiotemporal decorrelation and are therefore automatically excluded from processing based on coherence thresholding (Fig. 6). Due to insufficient ascending-track coverage in the Shugakuin area, the deformation analysis for the Shugakuin Imperial Villa was primarily based on descending-track data (Figs. 1d and 5B).

Histograms of the estimated uncertainties in the ascending and descending LOS deformation rates are presented in Fig. 5E. The uncertainties in the UD and EW directions were obtained by propagating the ascending and descending LOS uncertainties through the same geometric decomposition matrix as used for the velocity components^{49,50} (Fig. 5E). Additionally, deformation points were grouped into build-up and vegetated areas within the cultural heritage area. For the ascending-track results, the mean uncertainty was estimated at 0.141 ± 0.037 mm/yr in vegetated areas and 0.128 ± 0.034 mm/yr in build-up areas; for the descending-track results, the corresponding values were 0.119 ± 0.035 mm/yr and 0.104 ± 0.031 mm/yr. In the vertical direction, the mean uncertainty was 0.119 ± 0.028 mm/yr in vegetated areas and 0.115 ± 0.022 mm/yr for built surfaces. Owing to the application of coherence thresholds during processing, the absolute differences are relatively small; however, uncertainties in vegetated areas are consistently higher than those in built-up areas. This observation aligns with previous studies indicating that vegetation cover reduces InSAR coherence and increases velocity uncertainty^{51,52}. In addition, within densely vegetated zones of the gardens, temporal decorrelation and related factors may further reduce InSAR coherence, potentially leading to conservative deformation estimates or data gaps. This phenomenon has been reported in several studies focusing on vegetated areas^{53,54}. In this study, the main deformation zones discussed are largely located on relatively stable artificial landscape features (e.g., buildings and paved surfaces), where vegetation effects are limited; nonetheless, potential interference cannot be entirely excluded. This represents one of the limitations of the present study. Future efforts could incorporate L-band SAR data or precise leveling measurements within the gardens would be valuable for further verification and refinement of the results.

Table 2 presents the RMSE values comparing InSAR-derived vertical velocities with GNSS measurements from 2020 to 2021. Supplementary Fig. S1 illustrates the representativeness of the GNSS stations in subsiding and stable zones. Four GNSS stations were available within the study area, representing different deformation regimes: KWBP and CKF are located in a

relatively stable zone; CNUJ lies within a subsiding zone; and KST is located in a periodic subsiding zone. The results demonstrate good agreement between the two datasets. For instance, at the KWBP site, accuracy improved by ~43% when ascending and descending tracks were combined, compared to using only ascending-track data. Overall, the precision improved by ~36% compared to using only the descending track. Minor discrepancies were, however, observed at other stations and in the aggregated comparison. Owing to restrictions on installing GNSS stations within Kyoto culturally sensitive traditional garden heritage and historical urban landscape areas, only four public GNSS stations are available within the city. In addition, precise leveling or maintenance records are difficult to access. Consequently, validation based on only these four stations may be insufficient, representing a limitation of this study. Local discrepancies may therefore arise when comparing site-specific deformation with city-wide trends.

Given that subsidence rates are typically reported in integer millimeters per year, this study defined subsiding pixels as those exhibiting an annual vertical displacement rate of ≤ -2 mm/yr, where negative values indicate subsidence. This conservative threshold accounts for potential local deviations and aligns with the upper range of typical InSAR measurement uncertainties. These criteria are consistent with accuracy ranges reported in previous studies^{16,17}.

Main subsidence area

During the monitoring period from 2017 to 2021, the main subsiding areas within the garden heritage site were identified based on vertical velocity estimates derived from combining ascending and descending track data.

At the Kyoto Imperial Palace, subsidence was identified within the Shishinden building complex. Notable subsidence was observed near the northern part of the main hall and around the corners of the eastern auxiliary buildings (Fig. 6a). The Shishinden building complex spans ~4500 m², with the main hall occupying around 1500 m². No significant subsidence was observed in the Omiya Palace or the surrounding buildings within the Sento Imperial Palace during the observation period. Additionally, owing to dense vegetation in the water-feature areas, the number of high-coherence points was insufficient, precluding subsidence identification in these regions to date (Fig. 6b).

At Katsura Imperial Villa, subsidence was detected on Oyama Island, the largest artificial island formed through lake excavation and piling of excavated soil (Fig. 6c).

At Shugakuin Imperial Villa, subsidence was detected around the Guest Hall complex of the middle villa and adjacent retaining walls (Fig. 6d).

The next step focused on identifying the potential causes of subsidence by integrating construction methods with InSAR time series data and relevant contextual information.

Discussion

Three main factors contribute to LAND subsidence in these four imperial gardens. First, subsidence of traditional palace buildings and white sand courtyards may be attributed to Holocene depositional environments.

Before 794, the Kyoto Basin, in which Kyoto Gyoen is situated, frequently experienced flooding from its rivers. After the Heian period began, the reduction of floodplains allowed the aristocratic Reizei family established a garden within the present-day grounds of the Kyoto Imperial Palace during the Heian period (794–1185). The garden has become renowned for its use of spring water gushing from the ground as a key landscape feature. This site served as an imperial garden since 1331. After Tokugawa Ieyasu entered Kyoto in 1603, the area underwent large-scale expansion and infill construction, including the development of palace buildings and gardens. The fires of 1708 and 1788 caused extensive damage, resulting in the accumulation of burnt debris and flood-borne sediments across the site. Reconstruction took place in 1790. Another major fire in 1854 destroyed most of the palace complexes again. Reconstruction began in 1855, largely replicating the layout established during rebuilding in 1790. This reconstruction laid the foundation for most of the existing buildings, including the Shishinden. After the capital was moved to Tokyo in 1869, this site was

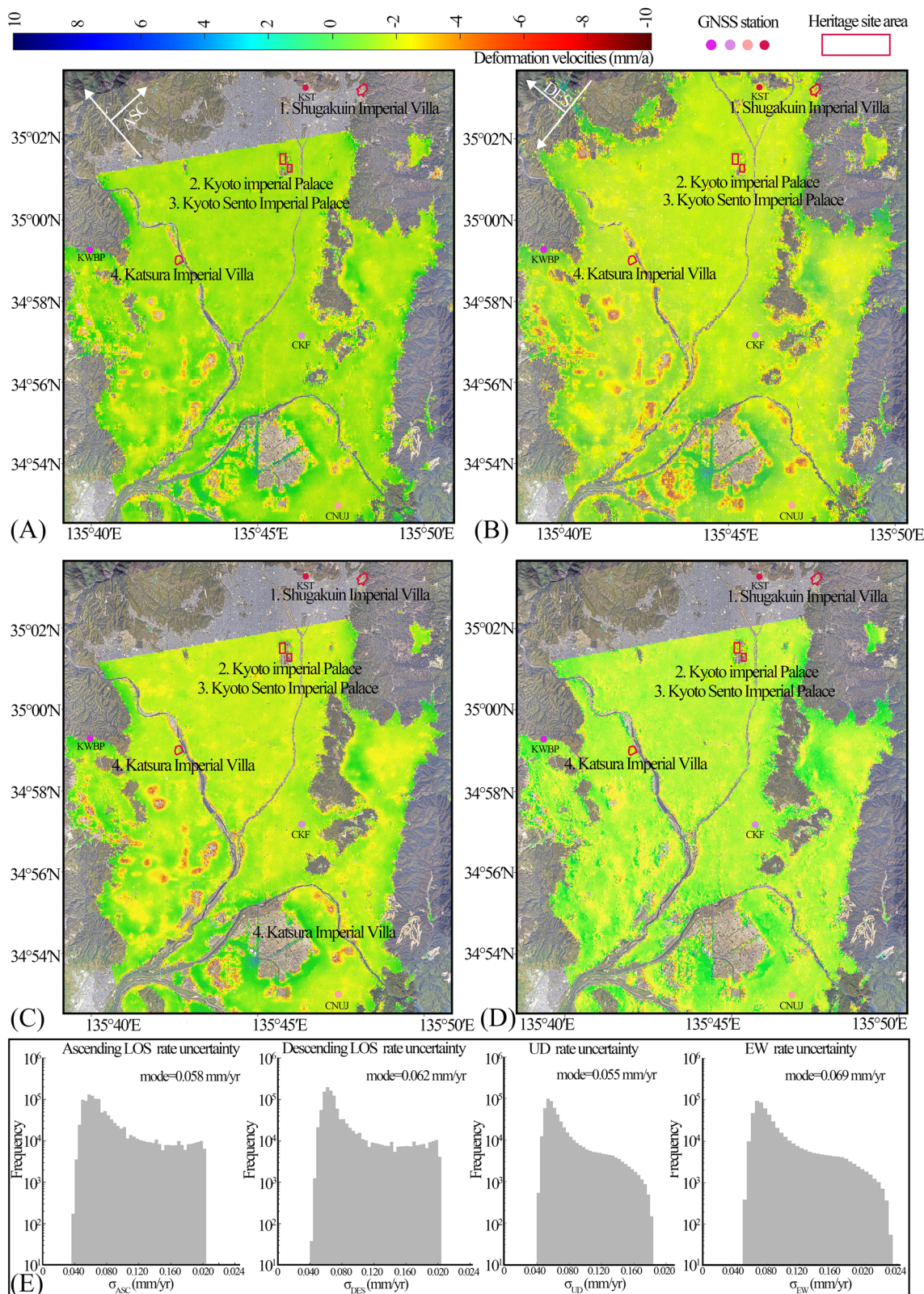


Fig. 5 | Vertical velocity map and uncertainty statistics. A, B Vertical velocities projected along the LOS direction from ascending and descending track data; C vertical velocity and D east–west velocity component derived from the

decomposition of LOS velocities. E Histograms of velocity uncertainty (mm/yr) for ascending LOS, descending LOS, UD, and EW components.

neglected. In 1877, the grounds underwent renovation through soil covering and regrading, accompanied by the construction of earthen and stone walls, as well as the development of roads around the garden. Since 1992, the Kyoto Imperial Palace has discontinued use of the Kamo River water supply

system established in 1912 and has switched to a groundwater system to support pond maintenance and landscape irrigation within the garden.

Based on InSAR results, several subsiding points were detected on the northern side of the main building and the corner areas of the auxiliary

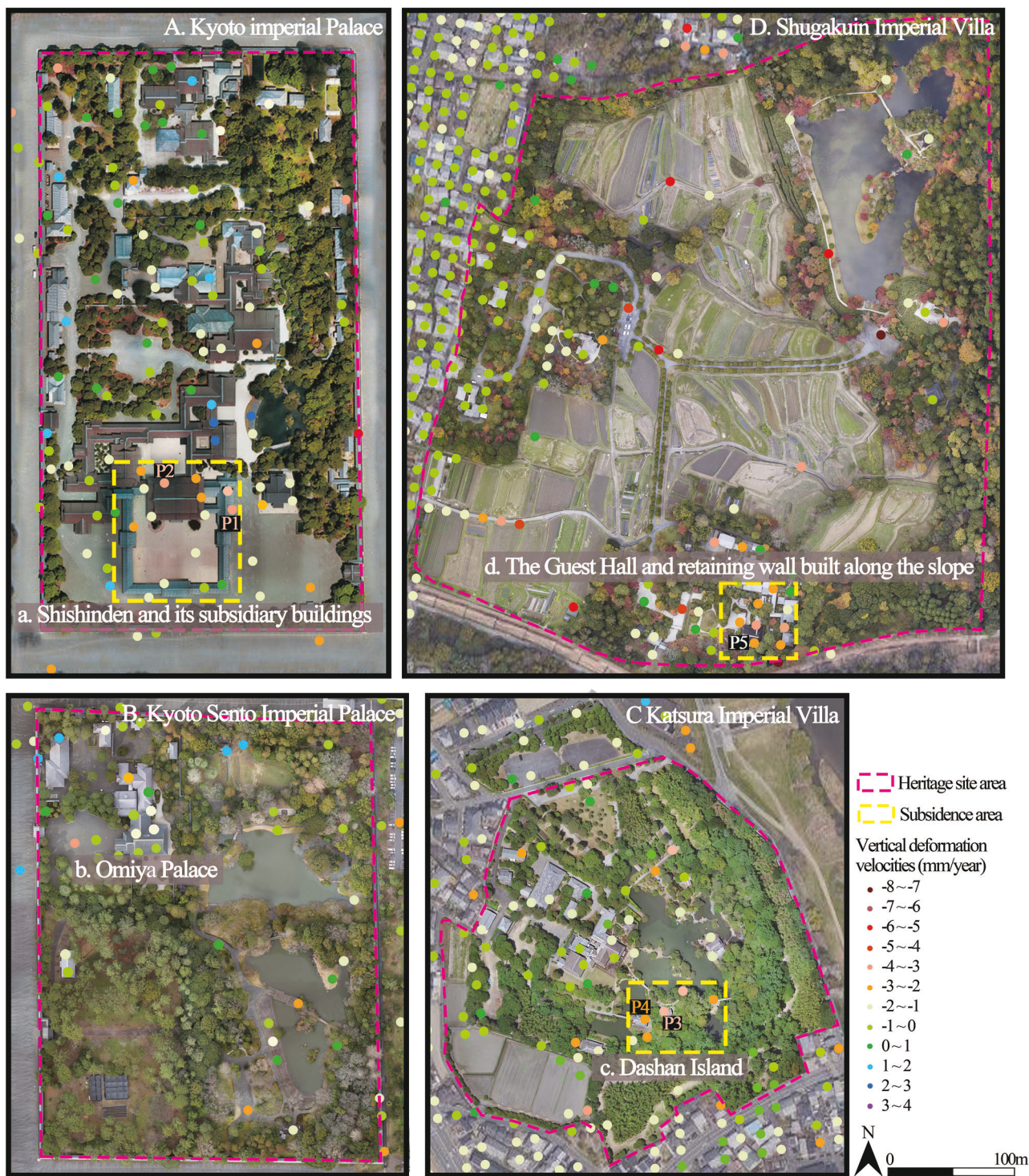


Fig. 6 | Major subsidence areas identified based on the decomposition of LOS velocity components. A Kyoto Imperial Palace. B Sento Imperial Palace. C Katsura Imperial Villa. D Shugakuin Imperial Villa.

buildings within the Shishinden building complex (Fig. 6A). Based on borehole investigation reports⁵⁵, traditional Japanese timber construction standards⁵⁶, and records on the conservation of cultural heritage buildings⁵⁷, a schematic cross-sectional diagram was drawn to illustrate the main structural composition of the representative Shishinden building complex and its surrounding courtyard within the Kyoto Imperial Palace (Fig. 7A). The schematic diagram represents the typical foundation construction methods and the subsoil composition of most palace buildings and white sand courtyard.

The building foundations employed traditional architectural techniques introduced from China, including the use of layered rammed-earth platforms. Foundation stones were placed above the platform to resist moisture and distribute the structural load evenly. The load was then transferred upward through the column bases and horizontal beams to the roof structure. The lower part of the foundation incorporates the kaku-tatami (grid raft) foundation method—a traditional Japanese technique introduced during the 1855 reconstruction to enhance seismic stability.

The courtyard section primarily features a surface layer ~2–3 cm thick of white sand, underlain by a leveling layer composed of either clean sand or mixed sandy soil, and a lower layer of compacted foundation or gravel bedding to ensure proper drainage and structural stability. And the foundations of the buildings and courtyards are situated within thick Holocene deposits, consisting of clay, silt, and fine sand (Fig. 7A).

Numerous studies have shown that historical heritage sites constructed over many generations located on Late Pleistocene to Holocene environments—such as alluvial fan plains, lakes, marshes, and deltas—are prone to land subsidence. This is primarily due to the presence of thick Late Pleistocene to Holocene sediments in the subsoil, especially after artificial fill such

as successive platform reinforcements, post-disaster backfilling, and landscape ground leveling, which are susceptible to long-term land subsidence^{4,19,58}.

Unlike Katsura and Shugakuin Imperial Villa, where small-diameter timber is commonly used to express lightness and natural beauty, the palace buildings of the Kyoto Imperial Palace are constructed with large load-bearing wooden columns made of Japanese cedar or fir, reflecting a sense of solemnity. The prolonged structural load, together with the Holocene depositional environment, may render the palace buildings susceptible to land subsidence. Field investigation revealed that at P1(the northeast corner of the Shishinden building complex) and P2 (north side of the Shishinden building) (Fig. 6a), long cracks have developed, and multiple visible cracks extend outward from the buildings across the platform base (Fig. 7C). According to official past repair reports, it has been confirmed that cracks in many palace buildings within the Kyoto Imperial Palace have been widening gradually over time.

To further investigate the deformation characteristics, the time series was analyzed based on Seasonal-Trend decomposition using Loess (STL). STL decomposition results show that the seasonal deformation component in the P1 and P2 areas is significantly negatively correlated with monthly rainfall, with an approximate one-month response lag (Fig. 7B). This indicates that intensive rainfall events, after recharging groundwater and increasing soil moisture content, can lead to delayed surface subsidence, a phenomenon may related to the time required for groundwater infiltration and pressure transmission^{59–61}. As rainfall infiltrates through the courtyard's white-sand pavement (originally designed to minimize surface water retention and allow rapid percolation) and the foundation cracks of building

Table 2 | Mean square error (RMSE) between SBAS InSAR-derived and GNSS-derived vertical velocities at each station from 2017 to 2021

Location	Symbol of Fig	RMSE in vertical velocities (UNIT:mm/yr)		
		UD 2D	UD ASC	UD DES
KWBP	•	0.562	0.983	0.392
GKF	•	0.872	0.510	1.328
GNUJ	•	0.742	0.427	1.030
KST	•	*	*	0.759
OBERALL		0.701	0.663	0.988

Data source: Sentinel-1 ascending and descending - ESA; GNSS – NGL; processed by the authors.

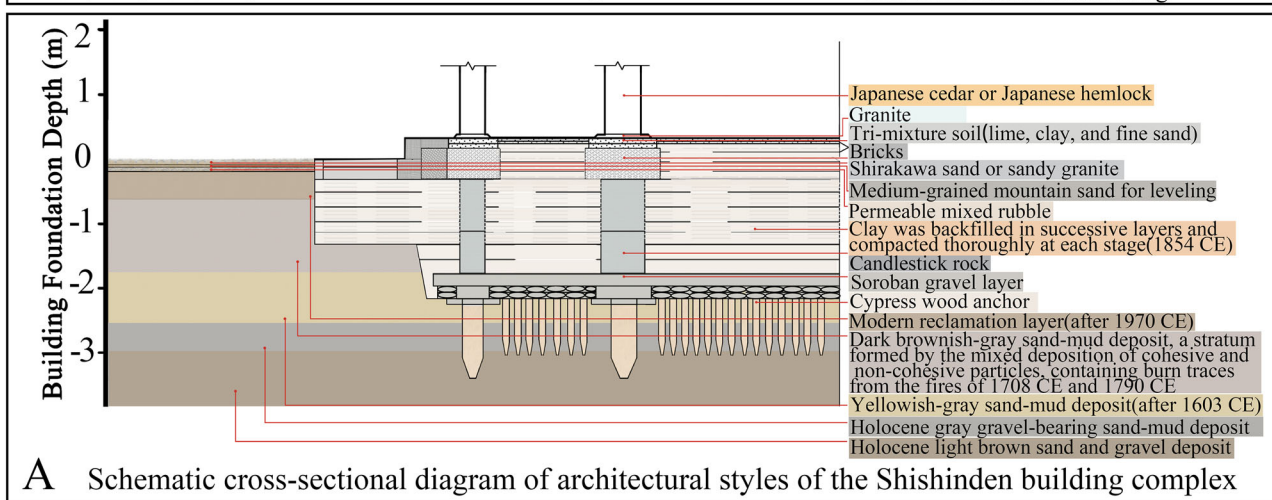


Fig. 7 | Schematic cross-section and deformation analysis within the Kyoto Imperial Palace. A Schematic cross-section of the foundation of the Shishinden building complex. B STL decomposition^{60,81} of monthly deformation–precipitation

and time series of points for P1(the northeast corner of the Shishinden building) and P2 (north side of the Shishinden building). C Field photographs of the P1 and P2 areas.

platforms into the underlying soil, it causes a sudden rise in pore-water pressure, which may accelerate the rate of subsidence^{62,63}.

The current conservation strategy follows the principle of “preserving existing conditions and respecting original materials.” Initial assessments are conducted through visual inspections to identify visible deterioration, such as cracks and structural collapse. Restoration is undertaken only when these issues are deemed to pose an evident threat to the building or the courtyard. During regular conditions, only minimal interventions are performed as part of routine maintenance. Consequently, bold splicing marks have appeared on some columns where no joints were originally required, or small metal nails and other materials have been added to maintain structural stability. It is recommended to inspect the structural damage and the elevation of column base stones within the affected area, and to implement preventive conservation measures in a timely manner to address limitations in current traditional restoration strategies. Furthermore, regular inspection of the drainage infrastructure surrounding the courtyards and palace buildings is advised, with particular attention given during the rainy season.

The Sento Imperial Palace is adjacent to the Kyoto Imperial Palace and shares similar historical development and stratigraphic characteristics (Fig. 1B). Initially used by aristocrats, the garden was constructed in 1630 by a retired emperor. Most buildings were reconstructed after a fire in 1855. The buildings within the Sento Imperial Palace are concentrated in the Omiya Palace complex, whereas the other areas contain relatively few artificial hardscape features (Fig. 6B). During this survey, it was observed that base reinforcements such as more *ne-maki kanamono* (metal fittings at column bases) were added to the main building of the Sento Imperial Palace, especially the Omiya Palace (Fig. 6a), and the Otsunegoten Building in the Kyoto Imperial Palace (Fig. 1a). Steel support tall columns were also installed under the eaves to enhance structural stability and prevent further subsidence or displacement. However, these reinforcements have, to some extent, compromised the classical landscape appearance of the gardens. In the reinforced areas, no significant subsidence was detected in the InSAR results (Fig. 6A, B).

Second, the subsidence observed in Katsura Imperial Villa may be caused by thick Holocene deposits beneath foundations constructed under lake excavation, hill construction, and stonework methods.

Katsura Imperial Villa is located on the west bank of the Katsura River and covers an area of 69,400 m². During the 10th–11th centuries, it served as a villa for the Fujiwara family. Owing to its slightly elevated riverine sandbar terrain and renowned moonlit scenery, it remained a favored retreat for aristocrats to enjoy moon viewing throughout the centuries. Around 1615, Prince Hachijō Toshihito began constructing the detached palace on this site, excavating lakes, hills constriction, building halls, and laying out stone-paved garden paths⁶⁴. By ~1662, the layout had nearly assumed its current form. Since its establishment, the buildings of the Katsura Imperial Villa have never suffered from fire, allowing the estate to preserve its historical appearance. The garden’s designers first excavated the Katsura River floodplain to create the “Gyokusui Pond.” The excavated soil was artificially backfilled nearby to form Oyama Island and two lingzhi-shaped central islets (also known as “Shinsen Islands”)⁶⁵. Oyama Island has a larger height and area than the other islets, making it the highest point in the garden, and it is surrounded by relatively deep pond water. In addition, during the construction of the garden, an “inner canal” was excavated on the eastern side of the site. The western side of this canal became the present-day Shōkintei area, which was largely preserved as a land area^{66,67}, with relatively shallow water surrounding it (Fig. 1c). At the highest point on the northern part of Oyama Island, a flower-viewing pavilion and its associated courtyard (P3) were constructed, while on the lower, flatter southern part of the island, a Garden Hall and its associated courtyard (P4) were built (Fig. 6c).

According to the InSAR results, a concentration of subsidence points was observed on Oyama Island. In contrast, the smaller central islands, primarily composed of vegetation and scattered stones for landscaping, had fewer high-coherence points; thus, no subsidence was detected (Fig. 6C). Based on the *Kyoto Katsura Imperial Villa Photographic and Surveyed Drawings Collection*, borehole investigation reports⁵⁵, records from the

Imperial Household Agency, and architectural preservation reports⁶⁸, cross-sectional diagrams were drawn illustrating the Flower Viewing Pavilion and Garden Hall, along with courtyard paving (Fig. 8A). It was found that the building and courtyard foundations are primarily situated on thick Holocene fluvial terrace deposits, which are highly compressible and may be prone to subsidence^{4,19,58}. The upper layer primarily consists of light-brown muddy sand and yellowish-brown clayey soil, which were artificially backfilled during the “lake excavation and piling of excavated soil” process. The lower layer comprises Late Pleistocene to Holocene fluvial terrace deposits, with localized intercalations of silt or clay layers. The overall stratigraphy presents an uneven interbedding of sand and mud. In the artificial landscape, the foundations are in direct contact with the sedimentary layers.

The foundation of the flower-viewing pavilion follows the typical *buseki-dodai-shiki* method, in which each column base rests directly on a large individual cornerstone (*kiso-ishi*). Crushed granite stones (*wari-kurii*) were used underneath for stabilization and drainage. At the base of the wall, crushed stones were similarly used as supports, with a neatly placed wooden sill above to bear the weight of the earthen wall (Fig. 8A1).

The foundation of the Garden Hall primarily employs a stone placement method, utilizing cut rectangular stones as individual cornerstones (*kiso-ishi*), upon which *dōsō-ishi* (top stones) are laid. Wooden columns were placed directly on top of the stones (Fig. 8A2). The foundation construction methods used for these two buildings have been widely applied in historical architecture within both the Katsura Imperial Villa and Shugakuin Imperial Villa. Moreover, their foundations did not adopt the *kaku-bari* (grid raft) foundation method, which became common in the 19th century to support heavier buildings, such as the Shishinden building in the Kyoto Imperial Palace, temple halls, or central palace structures⁶⁹.

The courtyard paving and garden path arrangements around the buildings were designed to harmonize with the architectural layout of the foundations. Before laying the paving stones, the landscape designer employs foundation techniques, similar to those used in building construction, by placing a layer of gravel as a bed to facilitate drainage. The upper stones are vertically embedded and closely interlocked with the underlying soil and gravel, forming a relatively stable structure. Mortar and cement are not used or permitted⁶⁹. This method is similar to the construction techniques used in the Arare-Koboshi path on the northern side of the Katsura Imperial Villa.

Past repair reports of the Katsura Imperial Villa indicate that due to rainfall and historical changes have contributed to land subsidence, resulting in unevenness or cracking of the stone paving surfaces made of gravel. Based on the relationship between the STL-derived seasonal deformation component and monthly rainfall, it is observed that, unlike the plains (P1, P2) and the low-lying Garden Hall area of the artificial island (P4), which exhibit a moderate negative correlation with rainfall with a lag of about one month—the hilltop area near the Flower Viewing Pavilion (P3) shows a weak positive correlation without significant delay. This suggests that during intense rainfall events, rapid infiltration into the sandy-clayey backfill may induce short-term wetting expansion, manifested as transient uplift, whereas more favorable drainage conditions than in lower-lying areas may prevent a significant lag effect. Similar phenomena have also been reported in previous studies^{70–72}. Based on field investigations, significant cracks have formed on the ground in front of the Garden Hall (Fig. 8B2, C2). At the Flower Viewing Pavilion, some small paving stones have become loosened, with several transverse cracks observed in the wooden columns (Fig. 8B1, C1).

Many reports have described the paving at the Katsura Imperial Villa as a refined yet fragile form of landscape art. In addition, during the major restoration project of the Showa era (1970s), the Garden Hall was identified as the structure most at risk of collapse and became the first building in Katsura Imperial Villa to undergo complete disassembly and large-scale restoration. In the future, more attention should be paid to the rainy season and the maintenance of stone paving surfaces.

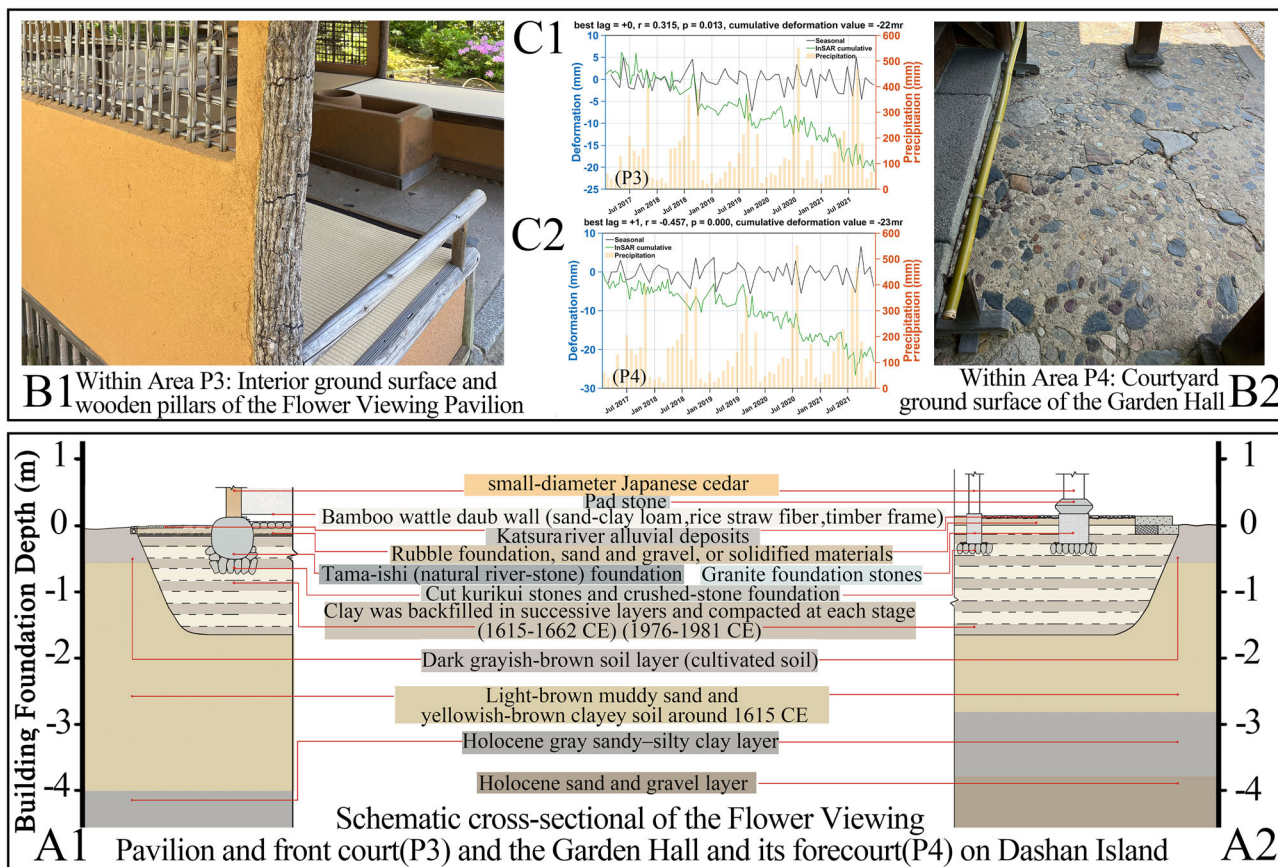


Fig. 8 | Schematic cross-section and deformation analysis within Katsura Imperial Villa. Schematic cross-section of the foundation of A1 The Flower Viewing Pavilion and A2 The Garden Hall buildings along with the courtyard paving. B Time

series and STL decomposition^{60,81} of monthly deformation–precipitation of points for P3 (The Flower Viewing Pavilion along with the courtyard) and P4 (The Garden Hall along with the courtyard paving). C Field photographs of P3 and P4 area.

Third, Subsidence at the Shugakuin Imperial Villa may be caused by Groundwater gushing under terrain-dependent garden construction methods.

The Shugakuin Imperial Villa is located at the southwestern foot of Mount Hiei and was constructed between 1656 and 1659 as a hillside estate. It leverages the natural terrain and surrounding expansive rice fields, organizing the upper, middle, and lower villas into a unified landscape composition (Fig. 1d). Among the four gardens, Shugakuin Imperial Villa possessed the most abundant water resources. Situated at the base of Mount Hiei, the villa benefits from year-round groundwater flow throughout the mountainous area. Rainwater and other surface water sources can rapidly percolate through the gravelly sand layers, while deep fractures in the underlying granite bedrock facilitate upward groundwater recharge into the area. The primary source of water for the Goryu Pond in the Upper Villa is two waterfalls diverted from the Otowa River.

Compared to the other three gardens, the area surrounding the Shugakuin Imperial Villa has not been heavily impacted by large-scale urbanization⁷³. In contrast, the Katsura Imperial Villa formerly had natural groundwater outflows, but 20th-century urban development and riverbed modifications caused groundwater levels to drop, resulting in the loss of springs such as the Katsura-no-Izumig. Historically, the Kyoto Imperial Palace and Sento Imperial Palace had natural spring outflows; however, due to subway construction and other developments, the groundwater level has declined. Today, the groundwater table in the Imperial Palace area lies ~9 m below the surface, and no spring outflows have been observed.

Based on the InSAR descending track detection results, a concentration of subsiding points was identified in the Guest Hall complex of the Middle Villa (P5) (Fig. 5D). Based on the *Kyoto Shugakuin Imperial Villa Photographic and Measured Drawings*⁷⁴, along with the 28.9-meter-deep borehole

investigation reports⁷⁵, a cross-sectional diagram of the foundation of the Guest Hall building and the surrounding retaining wall was drawn (Fig. 9A). It was found that beneath the landscape foundation lies a traditional unreinforced stone masonry retaining wall, which makes full use of elevation differences to place Irregularly shaped, naturally occurring blocky stones that have not been artificially cut for scenic effect. The building and courtyard foundations are situated on a bedrock of natural stone. The use of many natural and crushed stone (kuriishi) backfills allowed rainwater to infiltrate quickly, preventing water accumulation around the base of the wooden columns. Beneath the artificial foundation layer, the strata are primarily composed of alternating layers of gravelly coarse sand and fine sand (partly interbedded with silt) underlain by a granite bedrock. The highly permeable gravelly coarse sand layers and the relatively less permeable fine sand layers form a differential permeability interface, which may easily give rise to groundwater gushing within the water-abundant environment of the villa^{27,76}. This issue is frequently noted in the repair reports of the Shugakuin Imperial Villa, which highlight that foundational parts of buildings and courtyards are prone to damage due to prolonged disturbance of pore water pressure caused by groundwater.

The STL analysis results show that the seasonal deformation component at P5 is significantly positively correlated with monthly rainfall and is nearly synchronous (Fig. 9B). This suggests that the drainage and infiltration processes within the stony foundation pads and bedrock fractures beneath the structures are rapid, and that intense rainfall events may trigger surface deformation within a short time through infiltration and pore-pressure changes^{77,78}. Combined with the time series (Fig. 9B), this area exhibits cyclical land subsidence patterns, characterized by uplift during the rainy season as groundwater levels rise and subsidence before and after the rainy season ends. Meanwhile, an InSAR study conducted from 2014 to 2020

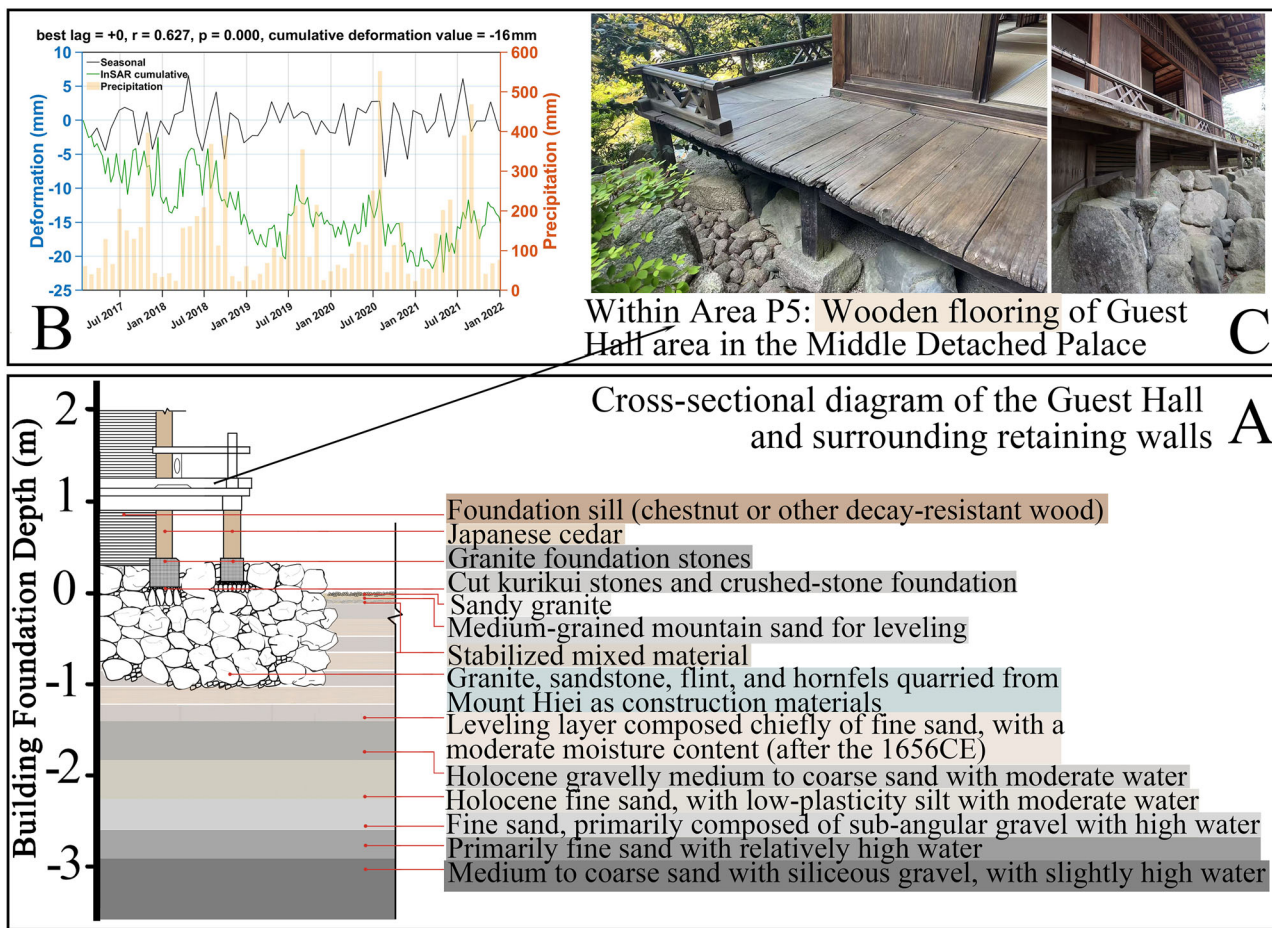


Fig. 9 | Schematic cross-section and deformation analysis within Shugakuin Imperial Villa. A Schematic cross-section of the foundation of (P5) the Guest Hall building and the surrounding retaining wall. B Time series and STL decomposition^{60,81} of monthly deformation–precipitation for P5. C Field photographs of P5 area.

across 73 cities in Japan found that many regions exhibited annual cyclical land deformation^{79,80}.

Field investigations revealed that the wooden flooring on the outer side of the Guest Hall has become loose and uneven (Fig. 9C). In the future, management and monitoring of this area should be enhanced during and around the rainy season. Additionally, the Lower Villa underwent repairs work in 2016–2017 due to damage to the revetment caused by groundwater seepage. No significant subsidence has been detected in this area during the InSAR monitoring period. As for the Upper Villa and other areas, the current available monitoring points are relatively scattered (Fig. 6D and 1D).

With respect to the limitations of this study, it should be acknowledged that the parameter settings in this study (limiting the temporal baseline to 60 days and relaxing the coherence threshold to 0.3) improved the overall coherence and spatial density of measurable points but may also reduce the number of interferograms and introduce phase noise from low-coherence noise. This represents one of the study's methodological limitations, and future work is expected to address this issue through the use of higher-resolution data and other enhancements.

Additionally, PS-InSAR offers advantages over SBAS-InSAR in terms of accurate point identification and is generally able to establish a closer correspondence with GNSS stations. However, within the heritage sites investigated in this study, the number of persistent scatterers was limited, and their spatial distribution was uneven due to vegetation cover and water bodies. Therefore, under improved data acquisition conditions (e.g., TerraSAR-X imagery) and suitable research objectives, the combined use of PS and SBAS methods, together with GNSS observations, represents a promising direction for future improvement, enabling both spatial coverage and high point-level accuracy to be achieved.

Previous InSAR-based studies on world cultural heritage sites such as Myanmar and China^{19,20,48} speculated that for heritage sites founded on soft soils, annual subsidence rates of 3 mm indicate medium levels of subsidence, often accompanied by cracks that reveal the instability of structural components. For most types of heritage foundations, subsidence rates exceeding 5 mm/yr are considered to reflect abnormal deformation, while rates reaching 10 mm/yr were considered to imply pronounced instability that poses a significant threat to heritage preservation. Under the current management strategy for garden heritage sites, which emphasizes “preservation of the present state with minimal intervention,” most subsiding heritage sites exhibit deformation rates in the range of 2–6 mm/yr. In particular, in areas underlain by soft soils, obvious cracks can be observed, and local measures such as supporting pillars and small steel nails have been installed; no large-scale restoration has been undertaken. Nevertheless, whether a single numerical threshold can clearly define the relationship between annual subsidence rates and structural stability remains uncertain. The severity of damage may vary depending on factors such as foundation conditions and the cumulative duration of subsidence and thus requires further investigation in future studies.

In terms of data, since groundwater data in most regions of Japan are confidential and not publicly available, and relevant exploration data are also lacking, this study was unable to further elaborate on the related conclusions using such data. It is hoped that future research will provide more in-depth explanations as more information becomes accessible.

In conclusion, first, this study employed multi-track InSAR data integration and remote sensing technique to monitor deformation and detect land subsidence spatial characteristics within four representative imperial gardens in Kyoto. The research results confirm

existing knowledge and are supported by the data. The study aims to explore the driving factors of land subsidence in Kyoto imperial garden heritage sites under historical landscape construction practices. The results indicate that subsidence may occur under the foundation construction methods of Kyoto palace buildings and white sand courtyard due to their foundation on Holocene sedimentary environments that have been repeatedly altered through generations of artificial filling. Subsidence may be triggered by the presence of thick Holocene deposits under lake excavation, hill piling, and stone masonry construction techniques; and in terrain-dependent garden designs, subsidence may be triggered by interference from underground water. The complex interplay between human historical activity and natural geographical conditions has shaped the construction methods and unique landscape heritage of gardens. As the landscape heritage evolves over time and outer hydrological conditions change, landscape heritage may be affected by the construction methods and geographical soil settings, and land subsidence may occur in this area.

Second, within a broader international context, subsidence phenomena have also been observed in other World Heritage gardens, such as the Summer Palace and Villa d'Este. These heritage sites are situated on shallow foundations and Holocene sedimentary units, where the long-term interplay of anthropogenic activities and natural factors makes localized ground instability likely to occur. Although the hydrogeological conditions differ across regions, preventive subsidence monitoring has become a shared necessity for heritage conservation.

Third, for the royal heritage sites examined in this study, efforts should focus on strengthening management and preventive protection during the rainy season. It is necessary to promptly repair ground fissures and extensive cracking in wooden columns to prevent further aggravation of structural instability.

Data availability

No datasets were generated or analysed during the current study.

Received: 9 June 2025; Accepted: 18 November 2025;

Published online: 05 December 2025

References

- Shigemori, K. *Zoen-Gaku Gairon* (Asakura Publishing, 1971).
- Shigemori, M. *Nihon Teien Shi Taikei* (Inoue Shoin, 1971).
- Zhang, J. *Neixin de Tingyuan: Riben Chuantong Yuanlin Yishu* (Zhongguo Jianzhu Gongye Chubanshe, 2006).
- Cui, J., Cui, S., Zhang, J. & Sun, F. Spatial characteristics of land subsidence in architectural heritage sites of Beijing's royal gardens based on remote sensing. *Heritage* **8**, 113 (2025).
- Park, J. Y. A study of planning for Gumswee-dong garden heritage maintenance. *J. Korean Inst. Tradit. Landsc. Archit.* **33**, 41–51 (2015).
- Zeayter, H. & Mansour, A. M. H. Heritage conservation ideologies analysis – Historic urban landscape approach for a Mediterranean historic city case study. *HBRC J.* **14**, 345–356 (2018).
- Brown, A. *The Genius of Japanese Carpentry: Secrets of an Ancient Woodworking Craft*, 2nd ed. (Tuttle Publishing, 2014).
- Ding, Y. & Zueva, P. A traditional Japanese garden and its lessons for modern times. *Landscape Archit. Art.* **19**, 85–97 (2021).
- Martínez de Arbulo, A. The ship of theseus: a misleading paradox? The authenticity of wooden built heritage in Japanese conservation practice. *J. Archit. Conserv.* **28**, 151–167 (2022).
- Brebbia, C. A. *Structural Studies, Repairs and Maintenance of Heritage Architecture XIII* (ed. Brebbia, C. A.) (WIT Press, Southampton, 2013).
- Zhang, J. et al. Processing of building subsidence monitoring data based on fusion Kalman filtering algorithm. *Alex. Eng. J.* **60**, 3353–3360 (2021).
- Sui, L., Zhu, H., Fang, C. & Zhai, S. Ground fissure monitoring based on 3D terrestrial laser scanning techniques. In *2017 7th International Conference on Manufacturing Science and Engineering (ICMSE 2017)*. 67–71 (Atlantis Press, 2017).
- Liu, S. P. et al. Land subsidence monitoring in sinking coastal areas using distributed fiber optic sensing: a case study. *Nat. Hazards* **103**, 3043–3061 (2020).
- Bonali, E., Pesci, A., Casula, G. & Boschi, E. Deformation of ancient buildings inferred by terrestrial laser scanning methodology: the Cantalovo church case study (Northern Italy). *Archaeometry* **56**, 703–716 (2014).
- Dzurisin, D., Dzurisin, D. & Lu, Z. *Interferometric Synthetic-Aperture Radar (InSAR)*, 153–194 (Volcano Deformation: Geodetic Monitoring Techniques, 2007)
- Yang, K., Yan, L., Huang, G., Chen, C. & Wu, Z. Monitoring building deformation with InSAR: experiments and validation. *Sensors* **16**, 2182 (2016).
- Yan, H. et al. A method for correcting InSAR interferogram errors using GNSS data and the K-means algorithm. *Earth Planets Space* **76**, <https://doi.org/10.1186/s40623-024-01903-7> (2024).
- Xu, H., Chen, F. & Zhou, W. A comparative case study of MTInSAR approaches for deformation monitoring of the cultural landscape of the Shanhua section of the Great Wall. *Herit. Sci.* **9**, 71 (2021).
- Nappo, N. et al. Subsidence in como historic centre (Northern Italy): assessment of building vulnerability combining hydrogeological and stratigraphic features, Cosmo-SkyMed InSAR and damage data. *Int. J. Disaster Risk Reduct.* **56**, 102115 (2021).
- Chen, F. et al. Remote sensing-based deformation monitoring of pagodas at the Bagan cultural heritage site, Myanmar. *Int. J. Digit. Earth* **15**, 770–788 (2022).
- Li, M., Gao, X., Yang, M., Tang, L. & Tang, B.-H. Evaluating the stability of architectural heritage from the perspective of InSAR: a practical study on Jianchuan Ancient Town. *Herit. Sci.* **12**, 394 (2024).
- Zhu, M. et al. Hypothetical analysis of ground deformation and its effects on archaeological sites of the Silk Roads with SBAS-DInSAR: An exploratory application in Xi'an City, China. *J. Appl. Geophys.* **241**, 105816 (2025).
- Lou, Q. *Twenty Lectures on Ancient Chinese Architecture* (Sanlian Publishing Press, 2004).
- Fujii, Y. Survey of bio-degradation in the Amida-do Hall of Higashi-Honganji. *Hozon Kagaku* **50**, 183–193 (2011).
- Nishiyama, K. et al. Identification of typical synoptic patterns causing heavy rainfall in the rainy season in Japan by a self-organizing map. *Atmos. Res.* **81**, 258–272 (2006).
- Hashimoto, M. Ground deformation in the Kyoto and Osaka area during recent 19 years detected with InSAR. In *International Symposium on Geodesy for Earthquake and Natural Hazards (GENAH) (International Association of Geodesy Symposia*, Vol. 145 (ed, Hashimoto, M.) (Springer, 2016).
- Imperial Household Agency. *Basic Geological Survey Report for the Fire Prevention System Improvement Design Project at Shugakuin Imperial Villa* (Imperial Household Agency, 2021).
- Farr, T. G. et al. The shuttle radar topography mission. *Rev. Geophys.* **45**, 361 (2007).
- Chen, X., Chen, J. & Wang, G. Mining subsidence based on integrated SBAS-InSAR and unmanned aerial vehicles technology. *J. Ocean Univ. China* **24**, 113–129 (2025).
- Ferretti, A., Monti-Guarnieri, A., Prati, C., Rocca, F. & Massonet, D. InSAR principles-guidelines for SAR interferometry processing and interpretation. *19*, (2007).
- Zebker, M. S. & Chen, J. A robust method for selecting a high-quality interferogram subset in InSAR surface deformation analysis. *Geophys. Res. Lett.* **51**, e2024GL11339 (2024).
- Ashraf, T., Yin, F., Liu, L. & Zhang, Q. Land subsidence detection using SBAS- and Stacking-InSAR with zonal statistics and topographic correlations in Lakhra coal mines, Pakistan. *Remote Sens.* **16**, 3815 (2024).

33. Adhillah, M. F., Hakim, W. L. & Lee, S. Multitemporal analysis of land subsidence induced by open-pit mining activity using improved combined scatterer interferometry with deep learning algorithm optimization. *Sci. Rep.* **14**, 6311 (2024).
34. Tao, Q. et al. Accuracy verification and evaluation of small baseline subset (SBAS) interferometric synthetic aperture radar (InSAR) for monitoring mining subsidence. *Eur. J. Remote Sens.* **54**, 642–663 (2021).
35. Berardino, P., Fornaro, G. & Lanari, R. A new algorithm for surface deformation monitoring based on small baseline differential SAR interferograms. *IEEE Trans. Geosci. Remote Sens.* **40**, 2375–2383 (2002).
36. Ferretti, A., Prati, C. & Rocca, F. Permanent scatterers in SAR interferometry. *IEEE Trans. Geosci. Remote Sens.* **39**, 8–20 (2001).
37. Hooper, A., Bekaert, D., Spaans, K. & Arikan, M. Recent advances in SAR interferometry time series analysis for measuring crustal deformation. *Tectonophysics* **514–517**, 1–13, (2012).
38. Fuhrmann, T. & Garthwaite, M. C. Resolving three-dimensional surface motion with InSAR: constraints from multi-geometry data fusion. *Remote Sens.* **11**, 241 (2019).
39. Kalavrezou, I.-E. et al. Application of time series InSAR (SBAS) method using Sentinel-1 for monitoring ground deformation of the Aegina Island (western edge of Hellenic volcanic arc). *Land* **13**, 485 (2024).
40. Hanssen, R. F. *Radar Interferometry: Data Interpretation and Error Analysis*, 1st ed, Remote Sensing and Digital Image Processing (Springer Dordrecht, 2001). <https://doi.org/10.1007/0-306-47633-9>.
41. Suhadha, A. G. & Harintaka, H. Multidimensional displacement analysis of Semeru Volcano, Indonesia following December 2021 eruption from multitrack InSAR observation. *Earth Sci. Inform.* **17**, 1539–1552 (2024).
42. Hu, J. et al. Resolving three-dimensional surface displacements from InSAR measurements: a review. *Earth Sci. Rev.* **133**, 1–17 (2014).
43. Harintaka, Suhadha, A. G., Syetiawan, A., Ardha, M. & Rarasati, A. Current land subsidence in Jakarta: A multi-track SBAS InSAR analysis during 2017–2022 using C-band SAR data. *Geocarto. Int.* **39**, 1–20 (2024).
44. Samieie-Esfahany, S., Hanssen, R. F., van Thienen-Visser, K. & Muntendam-Bos, A. On the effect of horizontal deformation on InSAR subsidence estimates. In *Proceedings of the Fringe 2009 Workshop*, ESA SP-677 (ESA, 2010).
45. Rouyet, L., Lauknes, T. R., Christiansen, H. H., Strand, S. M. & Larsen, Y. Seasonal dynamics of a permafrost landscape, Adventdalen, Svalbard, investigated by InSAR. *Remote Sens. Environ.* **231**, 111236 (2019).
46. Blewitt, G., Hammond, W. C. & Kreemer, C. Harnessing the GPS data explosion for interdisciplinary science. *Eos* **99**, 1–2 (2018).
47. Cui, S. et al. Research on deformation evolution of a large toppling based on comprehensive remote sensing interpretation and real-time monitoring. *Remote Sens.* **15**, 5596 (2023).
48. Tang, P., Chen, F., Zhu, X. & Zhou, W. Monitoring cultural heritage sites with advanced multi-temporal InSAR technique: The case study of the Summer Palace. *Remote Sens.* **8**, 432 (2016).
49. Morishita, Y. & Kobayashi, T. Three-dimensional deformation and its uncertainty derived by integrating multiple SAR data analysis methods. *Earth Planets Space* **74**, <https://doi.org/10.1186/s40623-022-01577-y> (2022).
50. Talledo, D. A. & Saetta, A. A multi-level semi-automatic procedure for the monitoring of bridges in road infrastructure using MT-DInSAR data. *Remote Sens.* **17**, 2377 (2025).
51. Wei, M. & Sandwell, D. T. Decorrelation of L-band and C-band interferometry over vegetated areas in California. *IEEE Trans. Geosci. Remote Sens.* **48**, 2942–2952 (2010).
52. Villarroya-Carpio, A., Lopez-Sanchez, J. M. & Engdahl, M. E. Sentinel-1 interferometric coherence as a vegetation index for agriculture. *Remote Sens. Environ.* **280**, 113208 (2022).
53. Devlin, K. R. & Lohman, R. B. Evaluation of vegetation bias in InSAR time series for agricultural areas within the San Joaquin Valley, CA. *Earth Space Sci.* **12**, e2024EA004062 (2025).
54. Pawłuszek-Filipiak, K., Wielgocka, N., Tondas, D. & Borkowski, A. Monitoring nonlinear and fast deformation caused by underground mining exploitation using multi-temporal Sentinel-1 radar interferometry and corner reflectors: application, validation and processing obstacles. *Int. J. Digital Earth* **16**, 251–271 (2023).
55. Kyoto City Archaeological Research Institute. *Summary Report of Archaeological Investigations in Kyoto City: Fiscal Year 1981* (Kyoto City Archaeological Research Institute, 1982).
56. Ito, Y. *Shōmei: A Traditional Japanese Manual of Architectural Proportions* (Kajima Institute Publishing, Tokyo, 1971).
57. Yu, W., Gong, H., Chen, B., Zhou, C. & Zhang, Q. Combined GRACE and MT-InSAR to assess the relationship between groundwater storage change and land subsidence in the Beijing-Tianjin-Hebei Region. *Remote Sens.* **13**, 3773 (2021).
58. Matano, F., Sacchi, M., Vigliotti, M. & Ruberti, D. Subsidence trends of Volturro river coastal plain (Northern Campania, Southern Italy) inferred by SAR interferometry data. *Geosciences* **8**, 8 (2018).
59. Wang, L. et al. Lag response of groundwater to changes in water and sediment characteristics in the middle Yellow River. *J. Hydrol.* **629**, <https://doi.org/10.1016/j.jhydrol.2022.128048> (2024).
60. Li, X. et al. Delayed response of groundwater to multi-year meteorological anomalies. *J. Hydrol.* **603**, 127081 (2021).
61. Suddeepong, A., Chai, J., Shen, S. & Carter, J. Deformation behaviour of clay under repeated one-dimensional unloading-reloading. *Can. Geotech. J.* **52**, 1182–1192 (2015).
62. Lo, S. R., Karim, M. R. & Gnanendran, C. T. (2013). Consolidation and creep settlement of embankment on soft clay: prediction versus observation. In *Geotechnical Predictions and Practice in Dealing with Geohazards* (Ch. 6, pp. 77–94).
63. Li, J. et al. Spatiotemporal inversion and mechanism analysis of surface subsidence in Shanghai area based on time-series InSAR. *Appl. Sci.* **11**, 7460 (2021).
64. Xiong, S., Wang, C., Qin, X., Zhang, B. & Li, Q. Time-series analysis on Persistent Scatterer-Interferometric Synthetic Aperture Radar (PS-InSAR) derived displacements of the Hong Kong-Zhuhai-Macao Bridge (HZMB) from Sentinel-1A observations. *Remote Sens.* **13**, 546 (2021).
65. Konoe, N. *Ketei-ki (Record of the Katsura Pavilion)*. (Katsura Imperial Villa Administration Office, 1625).
66. Imperial Household Record Office. *Rokuen Nichiroku (Deer Garden Diary)*. *Edo period manuscript (17th–19th century)*. (Kyoto Imperial Household Archives).
67. Sekinishi, T. Study on the preservation of natural elements (water and trees) of historical environment focusing on the garden of Katsura imperial villa. *Bull. Minami Kyushu Univ.* **38A**, 39–46 (2008).
68. Kiyoyoshi, M. Architectural drawing of the Shōkatei pavilion at Katsura Imperial Villa (measured survey) (Katsura Imperial Villa Administration Office, 1905).
69. Inoue, A. & Matsumura, S. A study on the transition of foundations and sill plates in wooden detached houses: Focusing on urban examples from the 1940s. In *Summaries of Technical Papers of Annual Meeting, Architectural Institute of Japan (AIJ) 2000*, 715–716 (AIJ, 2000).
70. Kono, F. & Kubo, H. Countermeasures for frost heave in roadways. *J. Jpn. Soc. Mech. Eng.* **80**, 1296–1299 (2017).
71. Özer, I. E., Rikkert, S. J. H. & van Leijen, F. J. Sub-seasonal levee deformation observed using satellite radar interferometry to enhance flood protection. *Sci. Rep.* **9**, 2646 (2019).
72. Neely, W. R. et al. Characterization of groundwater recharge and flow in California's San Joaquin Valley from InSAR-observed surface deformation. *Water Resour. Res.* **57**, e2020WR028451 (2021).

73. Li, G., Zhao, C., Wang, B., Liu, X. & Chen, H. Land subsidence monitoring and dynamic prediction of reclaimed islands with multi-temporal InSAR techniques in Xiamen and Zhangzhou Cities, China. *Remote Sens.* **14**, 2930 (2022).
74. Tanaka, A. & Maeda, T. A study on the Shugakuin Imperial “villa” through the itinerary of retired Emperor Reigen. *J. Archit. Plann. AJ* **601**, 217–224 (2006).
75. Mitsuhashi, S. *Wayo Kairyō Dai Kenchikugaku (Great Treatise on Japanese and Western Architectural Reform)* (Ōkura Shoten, 1911).
76. Preene, M. The John Mitchell Lecture 2022: thinking conceptually about groundwater problems. *Q. J. Eng. Geol. Hydrogeol.* **58**, 497 (2024).
77. Johnson, C. W., Fu, Y. & Bürgmann, R. Seasonal water storage, stress modulation, and California seismicity. *Science* **356**, 1161–1164 (2017).
78. Hammond, W. C., Blewitt, G. & Kreemer, C. GPS imaging of vertical land motion in California and Nevada: implications for Sierra Nevada uplift. *J. Geophys. Res. Solid Earth* **121**, 768–788 (2016).
79. Gu, L. et al. Research on main geological factors controlling water gushing and sand gushing of underground engineering in water-rich sand layer. *Coal Sci. Technol.* **51**, 275–283 (2023).
80. Morishita, Y. et al. Nationwide urban ground deformation in Japan for 15 years detected by ALOS and Sentinel-1. *Prog. Earth Planet. Sci.* **10**, 66 (2023).
81. Jiang, Y. & Yu, X. Space-based long term condition monitoring of cold region pavement with PS-InSAR. *J. Infrastruct. Preserv. Resil.* **6**, 4 (2025).

Acknowledgements

The authors would like to thank Professor Shengli Tao of Peking University for his valuable support and coordination of this research project. And this research was funded by the All-Directional Innovation Creator, PhD. Project of Japan (grant number 240PT18040), the Japan Science and Technology Agency, and the National Social Science Foundation of China [20BZS118].

Author contributions

J.C., Y.R., and X.H. conducted the InSAR analysis, with X.H. providing key technical support; J.C. and Y.R. wrote the manuscript; J.Z., S.T., and Y.R. contributed essential documentation and construction information on the

restoration of traditional Japanese gardens; J.C., S.C. provided important repair records and construction documentation related to traditional Chinese building techniques; J.C., K.H. and Y.R., X.H. supported data collection; X.H., J.Z., and F.S. supervised the manuscript. All authors reviewed and approved the final version of the manuscript.

Competing interests

The authors declare no competing interests.

Additional information

Supplementary information The online version contains supplementary material available at <https://doi.org/10.1038/s40494-025-02205-9>.

Correspondence and requests for materials should be addressed to Fuhao Sun.

Reprints and permissions information is available at <http://www.nature.com/reprints>

Publisher's note Springer Nature remains neutral with regard to jurisdictional claims in published maps and institutional affiliations.

Open Access This article is licensed under a Creative Commons Attribution 4.0 International License, which permits use, sharing, adaptation, distribution and reproduction in any medium or format, as long as you give appropriate credit to the original author(s) and the source, provide a link to the Creative Commons licence, and indicate if changes were made. The images or other third party material in this article are included in the article's Creative Commons licence, unless indicated otherwise in a credit line to the material. If material is not included in the article's Creative Commons licence and your intended use is not permitted by statutory regulation or exceeds the permitted use, you will need to obtain permission directly from the copyright holder. To view a copy of this licence, visit <http://creativecommons.org/licenses/by/4.0/>.

© The Author(s) 2025